Supporting Information

5.1 Supplementary figures

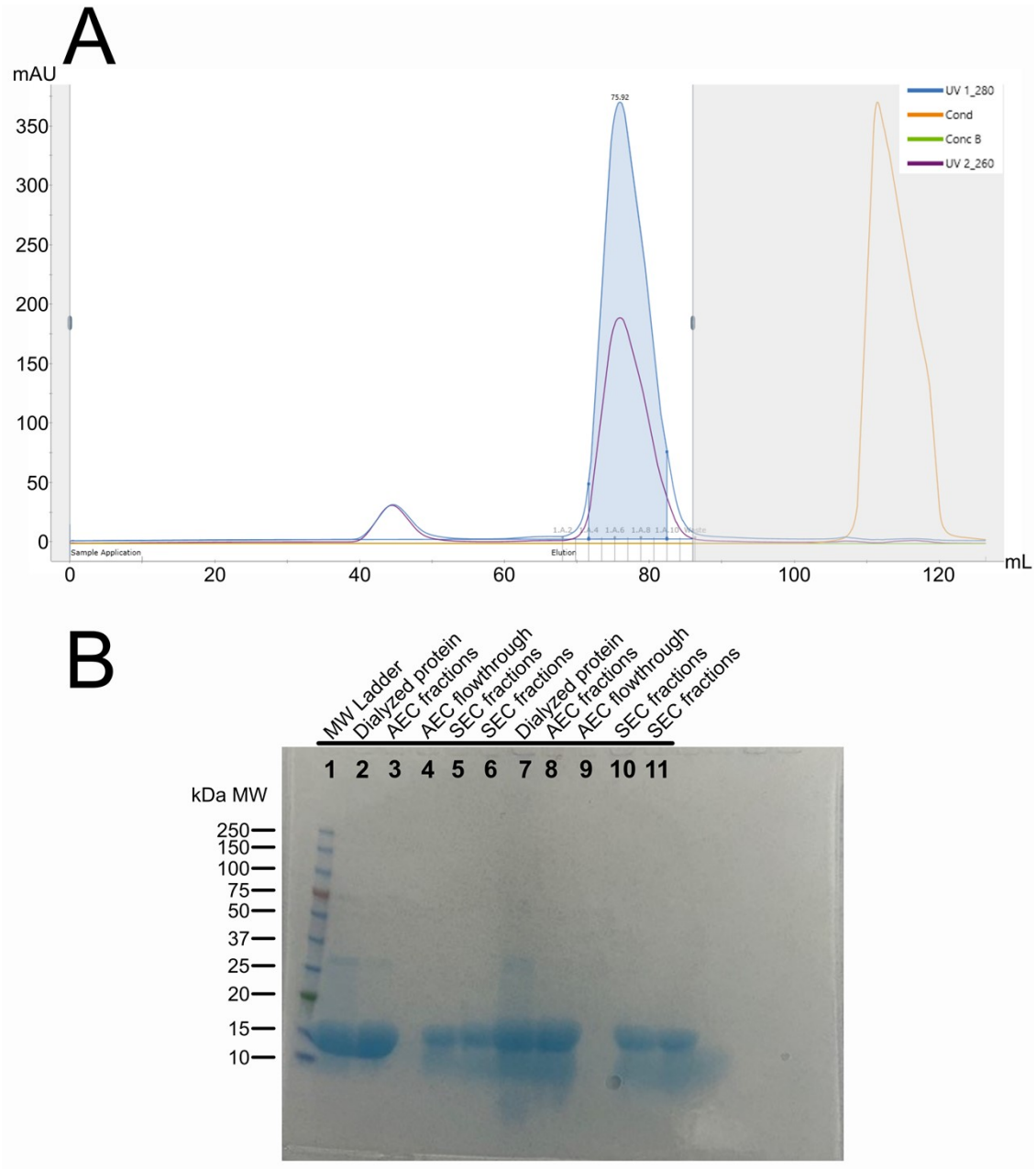

Fig. S1 Characterization of recombinant α-synuclein. A: SEC chromatogram - 280 nm absorbance in blue and 260 nm absorbance in purple. Blue shaded region marks fractions collected. B: SDS-PAGE gel of protein purification steps: Lane 1 - MW ladder (Precision Plus Protein™ Standards), lane 2 & 7 - dialyzed protein, lane 3 & 8 - collected fractions following AEC, lane 4 & 9 - AEC flow-through, lane 5, 6, 10 & 11 - collected fractions following SEC.

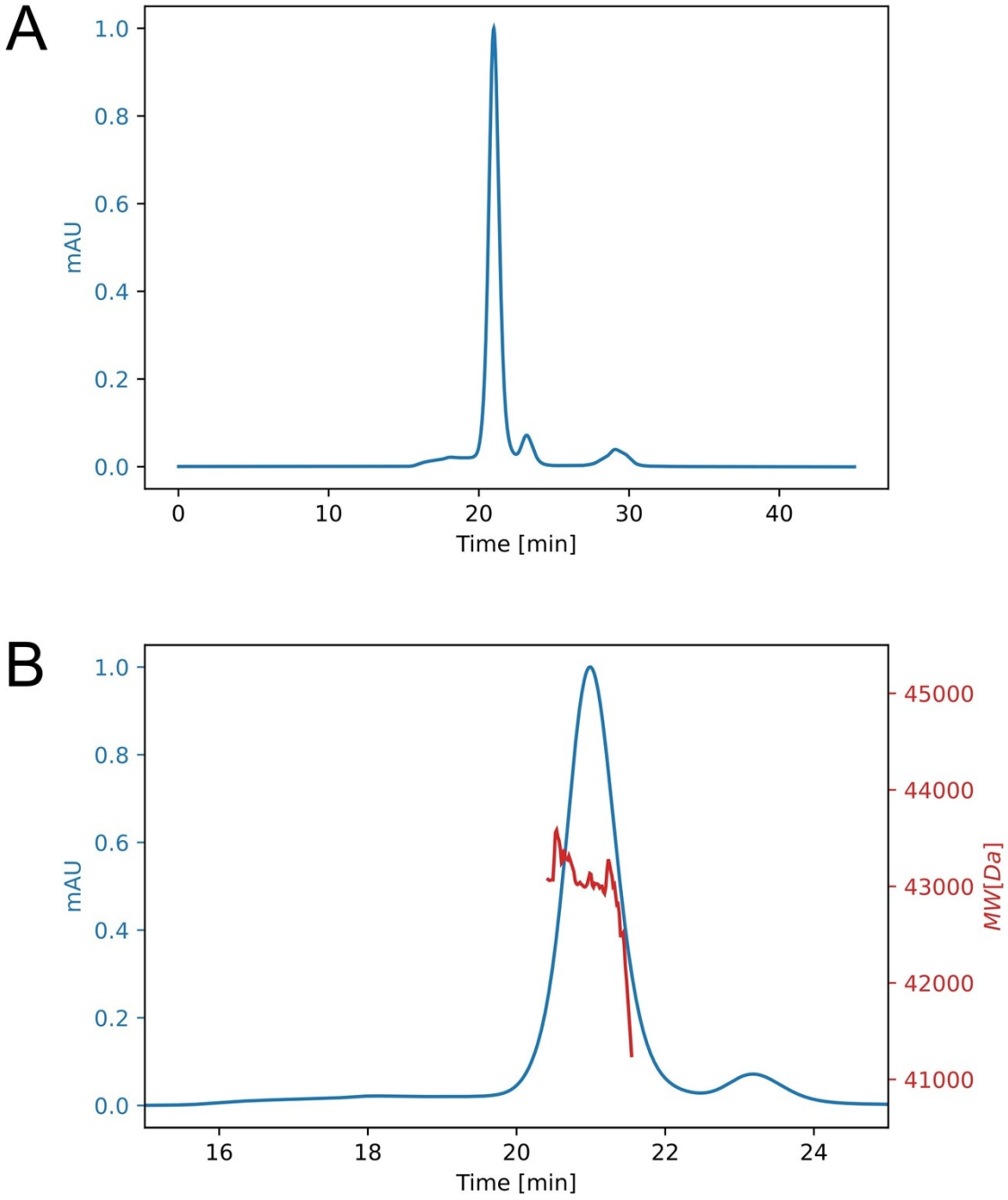

Fig. S2 Characterization of recombinant the NbSyn2-GFP construct. A:α-synuclein. A: SEC chromatogram - 280 nm absorbance. B: Sec chromatogram from A overlaid the MALS-measured molecular weight throughout the main peak (green). The mean MW across the peak is 42.96 kDa, in reasonable agreement with the expected MW of the final construct.

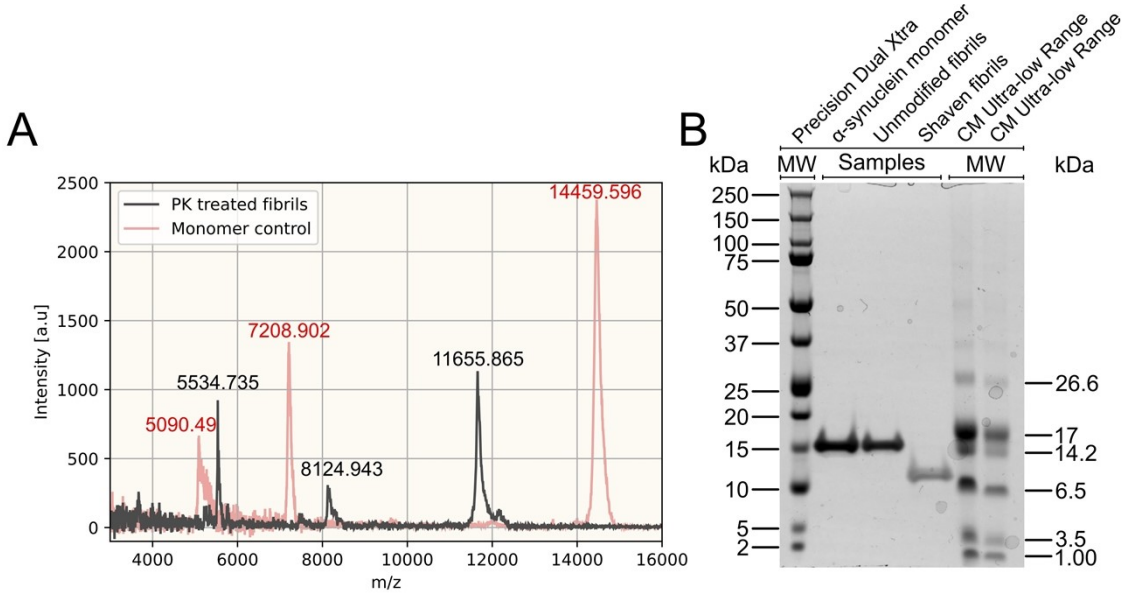

Fig. S3 Characterization of PK degradation of amyloid fibrils. A: MALDI-TOF spectrum of monomers released from PK-modified α-synuclein fibrils (black) and untreated monomeric α-synuclein (red). B: SDS-PAGE of monomers released from α-synuclein fibrils. Molecular markers used are Precision Plus Protein™ Dual Xtra and Color Marker Ultra-low Range (see method section). The left and right CM Ultra-low Range ladders vary only by load volume. Molecular masses of sample bands are calculated as the mean value evaluated from each molecular ladder.

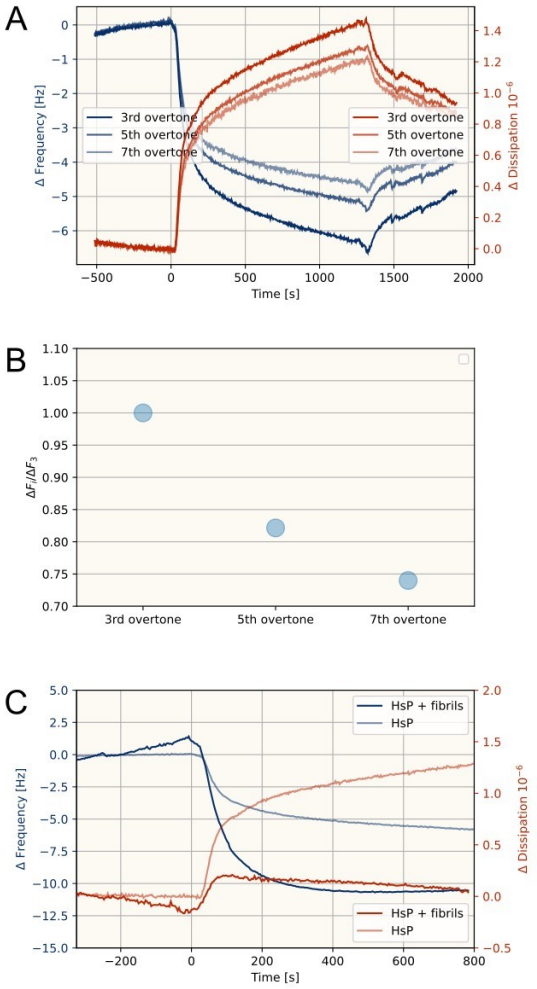

Fig. S4 Non-specific binding of HsP on a passivated QCM sensor. A: QCM-D analysis of 1 % HsP on a passivated sensor. HsP is injected at time 0 s, while washing with buffer starts at time 1200 s. The 3rd, 5th and 7th overtones are shown. B: Overtone dependence of HsP non-specific binding to the passivated QCM sensor. C: Comparison of the non-specific and fibril binding of HsP. The 3rd overtone is shown.

Non-specific binding of HsP to the sensor surface, as shown above, demonstrates characteristics distinctly different from binding of HsP to the fibril surface. Notably, the absolute dissipation to frequency ratio is much larger than observed for fibril binding (0.23 $10^{-6}/Hz$ compared to -0.03 $10^{-6}/Hz$), which is consistent with adsorption of protein to a soft PEG surface. Compatible with this observation, the adsorbed molecules can be removed, albeit slowly, with simple buffer wash. The unspecific binding also shows a significant overtone dependence, which is not observed in the presence of fibrils, similarly expected when molecules are not tightly bound to an immobilized fibril, but rather softly adsorbed onto a soft PEG surface. HsP also shows a significantly lower affinity for the sensor surface, compared to the amyloid fibrils, as shown in Fig. S4 C. Combined, this indicates that the majority of the binding signal observed for HsP in the presence of α-synuclein fibrils is likely to be binding to the fibril surface, rather than to the passivated sensor surface.

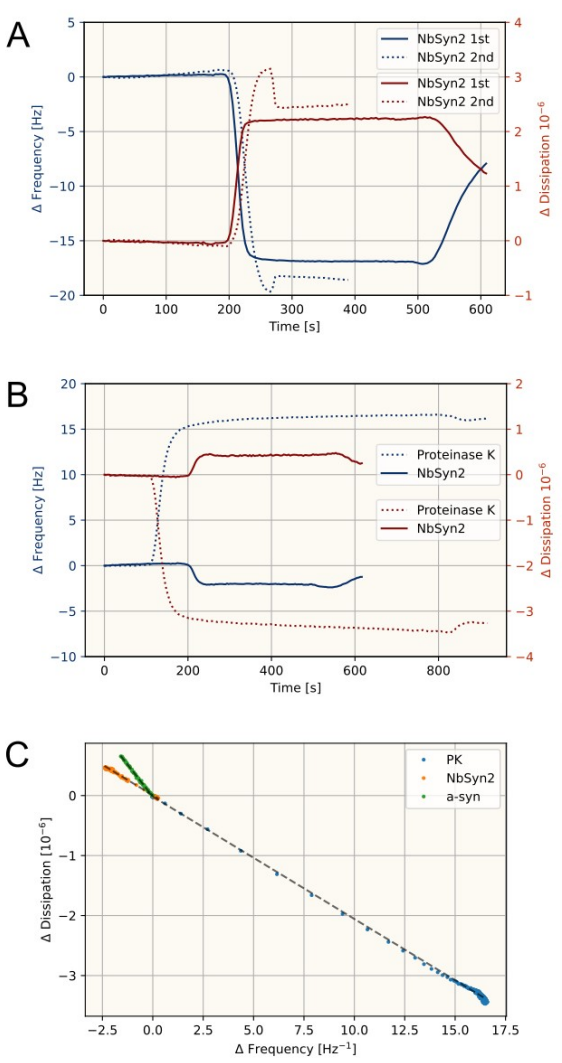

Fig. S5 Additional NbSyn2 data analysis. A: NbSyn2 binding data to untreated α-synuclein fibrils. B: PK incubation and subsequent NbSyn2 binding to α-synuclein fibrils. C: DF plot of NbSyn2 binding, fibril growth and PK shaving of α-synuclein fibrils.

NbSyn2 binds to un-modified α-synuclein fibrils. To demonstrate that NbSyn2 binding is inhibited by removal of the C-terminal region of the fibrils rather, than inhibition from the PMSF-wash, we incubated α-synuclein fibrils with NbSyn2 both before and after a PMSF wash. Fig. S5 A shows both incubation these periods, demonstrating both reversibility of the binding and that PMSF treatment does not interfere with NbSyn2 binding. NbSyn2 binding and shaving of the fibrils have the same DF-slope as fibril shaving by PK-incubation (-0.203 and -0.204 respectively).

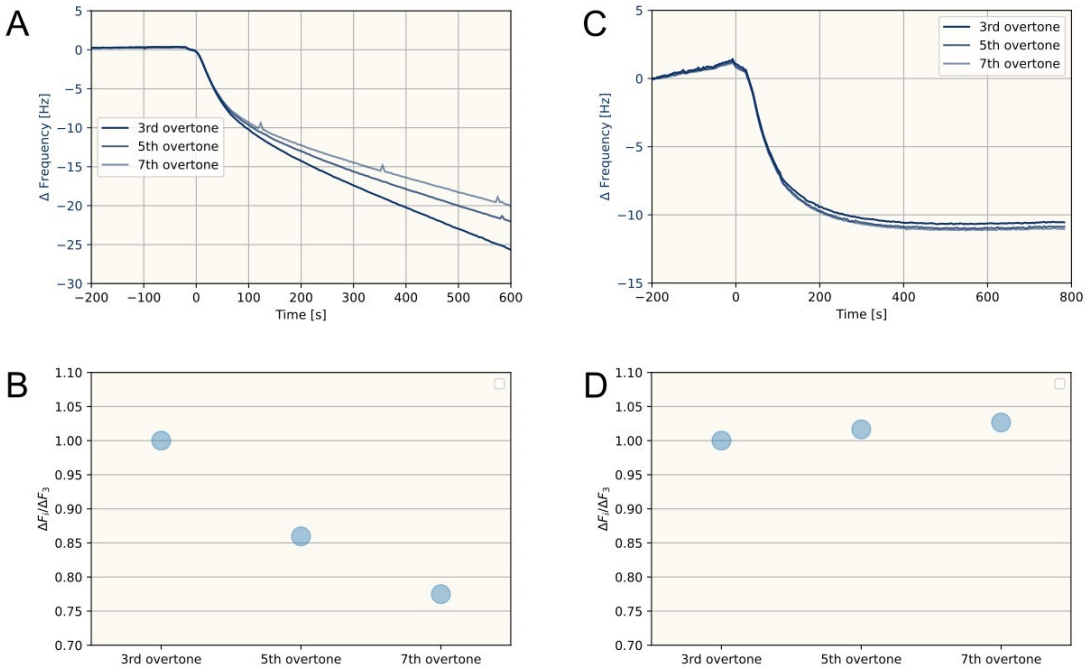

Fig. S6 Frequency overtone dependence of amyloid fibril growth and Hsp binding. A: Frequency response to amyloid growth, plotting the 3rd, 5th and 7th overtone. B: Relative magnitude of response to amyloid growth by the end of the growth period for the three overtones shown in A. C: Frequency response to HsP binding to fibrils, plotting the 3rd, 5th and 7th overtone. D: Relative magnitude of response to amyloid growth by the end of the growth period for the three overtones shown in C.

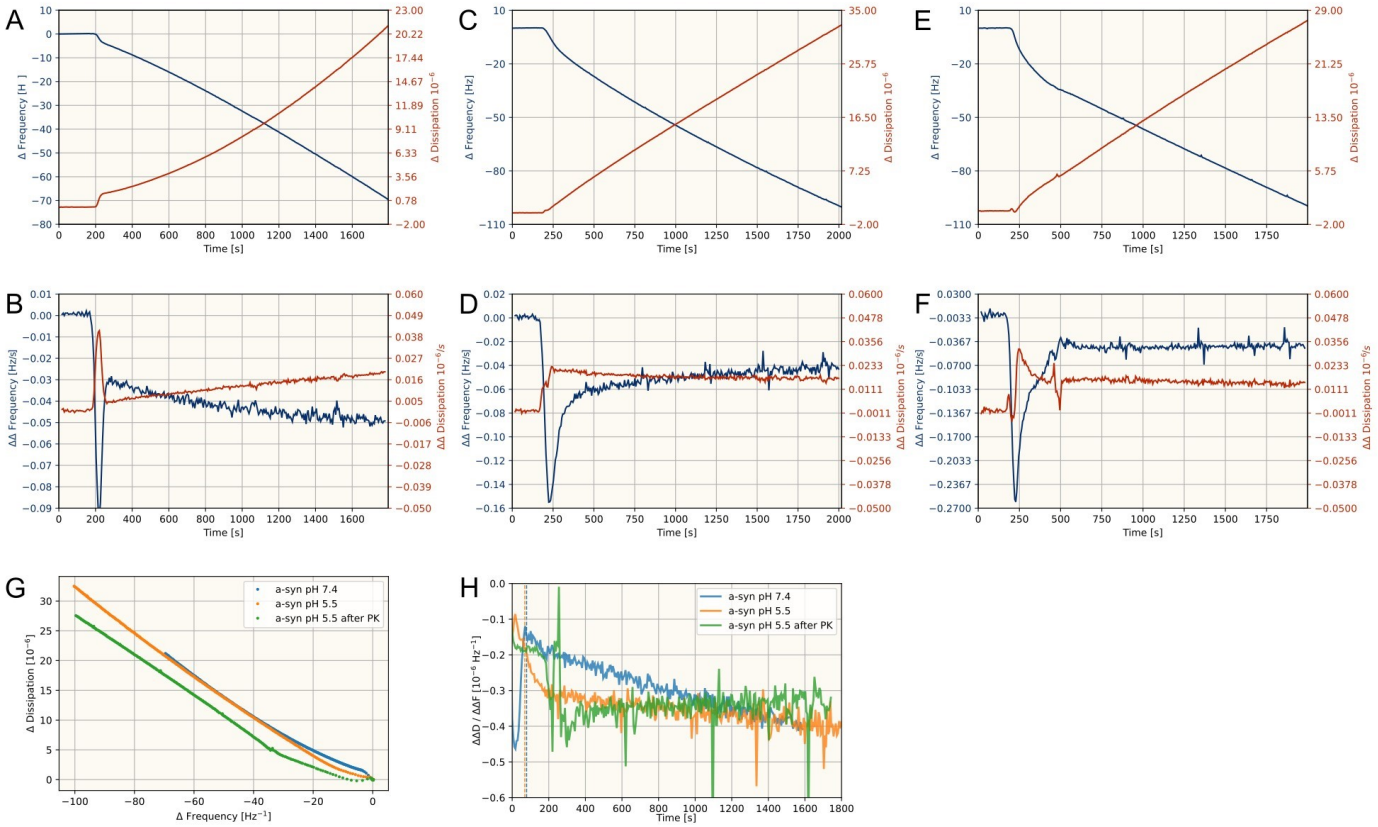

Fig. S7 QCM-D analysis of *α*-synuclein fibril growth as a function of pH on the same sensor. The 3rd overtone is plotted here. Fibrils are grown at pH 7.4, then 5.5, then Proteinase K treated and subsequently incubated at pH 5.5 again. A: *α*-synuclein fibril growth at pH 7.4. B: Numerical derivatives of A. C: *α*-synuclein fibril growth at pH 5.5. D: Numerical derivative of C. E: *α*-synuclein fibril growth at pH 5.5 after Proteinase K treatment. F: Numerical derivative of E. G: DF plot of A, C and E. In blue is the first *α*-synuclein growth period (pH 7.4), in orange is the following *α*-synuclein growth period (pH 5.5) and in green is the third *α*-synuclein growth period (pH 5.5) following Proteinase K treatment. H: Time-resolved DF plots of B, D and F using same color-coding as in G.

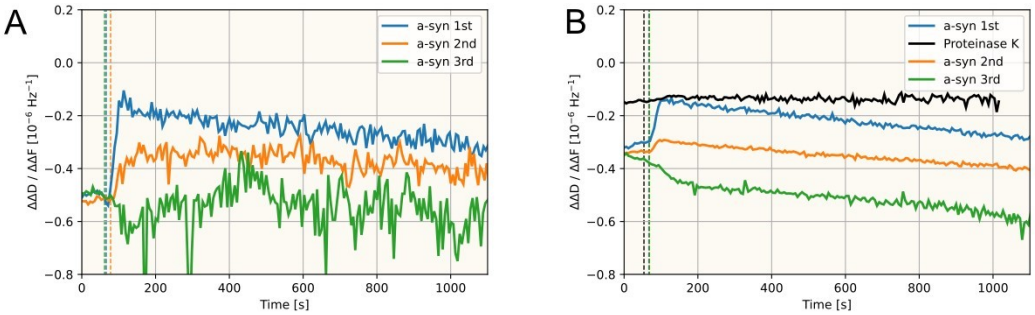

Fig. S8 Time-resolved DF plot, using the 3rd overtone, of α-synuclein fibril growth, with and without Proteinase K degradation. A: Time-resolved DF plot of Fig. 2 A/B. B: Timeresolved DF plot of Fig. 2 C/D. Proteinase K incubation occurs in between the first and second α-synuclein incubations. Both DF-plots show effectively a continuous decrease in DF ratio across all three growth phases, showing that the dominant mechanism of growth at the end of one growth period is also dominant at the beginning of the next growth period.

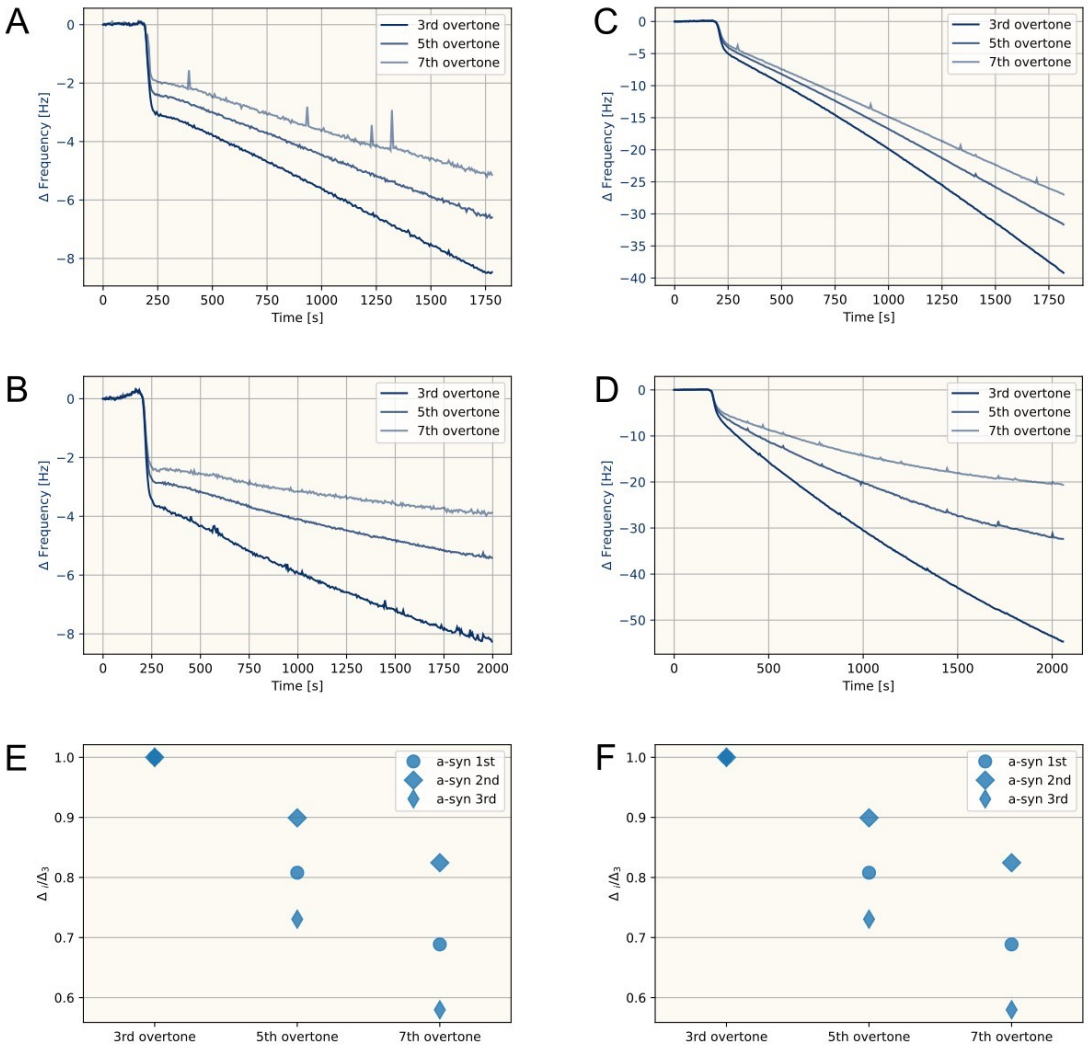

Fig. S9 Frequency overtone dependence of amyloid fibril growth with and without proteinase K treatment. A: Frequency response to amyloid growth of the 1st growth phase in Fig. 5 A, plotting the 3rd, 5th and 7th overtone. B: Frequency response to amyloid growth of the 4th growth phase in Fig. 5 A, plotting the 3rd, 5th and 7th overtone. C: Relative magnitude of response to amyloid growth by the end of the each growth period for the 3rd, 5th and 7th overtone of data from Fig. 5 A. D: Frequency response to Proteinase K degradation of the 1st shaving phase in Fig. 5 D, plotting the 3rd, 5th and 7th overtone. E: Frequency response to Proteinase K degradation of the 3rd shaving phase in Fig. 5 D, plotting the 3rd, 5th and 7th overtone. F: Relative magnitude of response to Proteinase K degradation by the end of the each shaving phase for the 3rd, 5th and 7th overtone of data from Fig. 5 D.

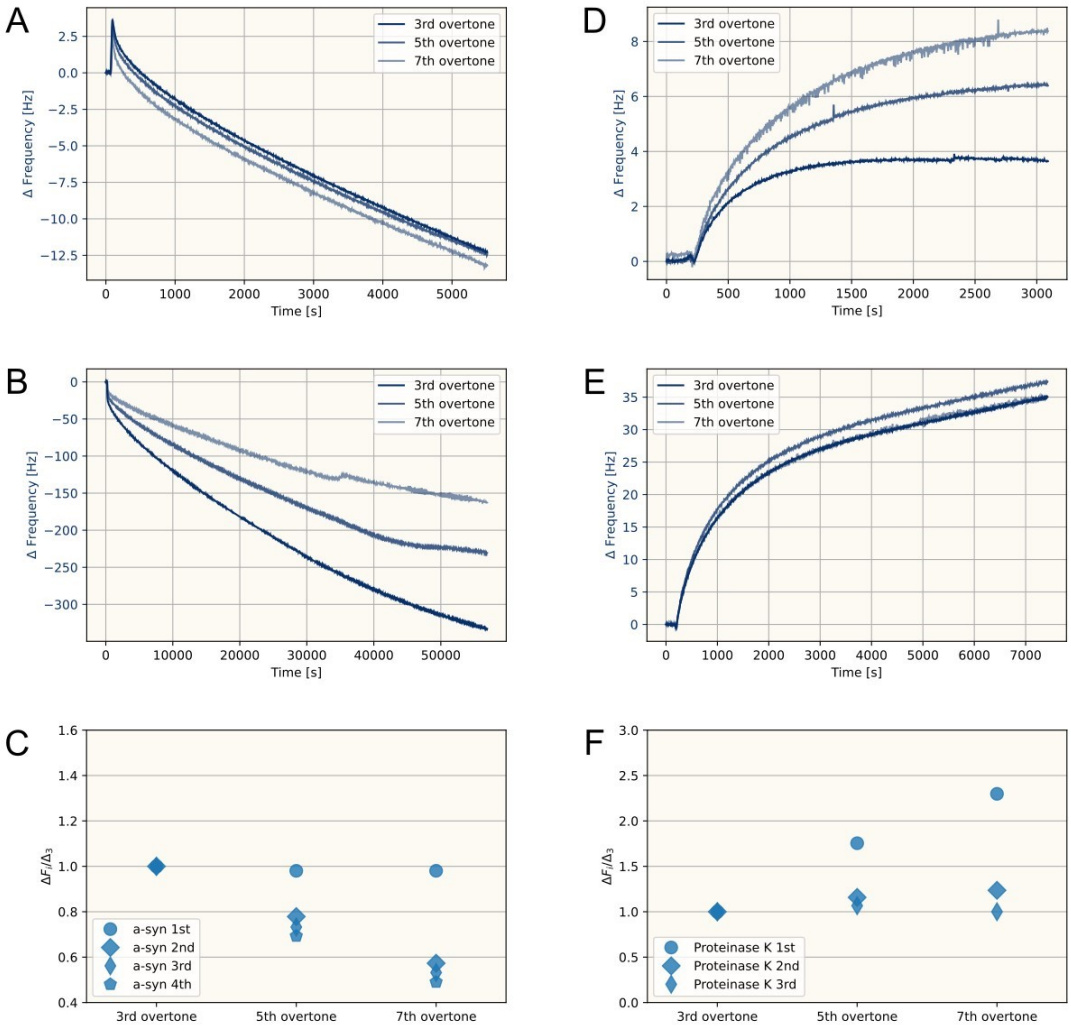

Fig. S10 Frequency overtone dependence of amyloid fibril growth and proteinase K treatment. A: Frequency response to amyloid growth of the 1st growth phase in Fig. 2 A, plotting the 3rd, 5th and 7th overtone. B: Frequency response to amyloid growth of the 3rd growth phase in Fig. 2 A, plotting the 3rd, 5th and 7th overtone. C: Frequency response to amyloid growth of the 1st growth phase in Fig. 2 C, plotting the 3rd, 5th and 7th overtone. D: Frequency response to amyloid growth of the 3rd growth phase in Fig. 2 C, plotting the 3rd, 5th and 7th overtone. E: Relative magnitude of response to amyloid growth by the end of the each growth period for the 3rd, 5th and 7th overtone of data from Fig. 2 A. F: Relative magnitude of response to amyloid growth by the end of the each growth period for the 3rd, 5th and 7th overtone of data from Fig. 2 C.

5.2 Kinetic models

Five kinetic models were created to model the QCM-D results, assuming different monomer-fibril interactions.

The parameters used for the models can be found in **Table S1**. As the values for most parameters are not directly determined each value has been approximated. A_{ext} is determined by calculating the surface area of the fibrillar part of one of the middle chains of an α-synuclein fibril (PDB 2N0A, chain E[1]). The surface area is calculated using DSSP[2].

Table S1 Parameters and variables used in the kinetic models of amyloid fibril growth.

Parameter	Value	Description
r_{sens}	0.0005 $molecule^{-1}$	Sensitivity loss by added mass
r_{shave}	0.5 $min^{-1} \cdot fibril\ end^{-1}$	Number of monomers added (x10^9) per fibril end (shaved fibril) per minute
r_{full}	0.05 $min^{-1} \cdot fibril\ end^{-1}$	Number of monomers added (x10^9) per fibril end (full-length fibril) per minute
r_{bind}	25 min^{-1}	Max number of monomers (x10^9) binding to the fibril surface per minute
r_{PK}	0.15 min^{-1}	Proteinase K degradation rate (x10^9) in molecules per minute
$A_{monomer}$	64.2 nm^2	Fibril surface area occupied by single monomer
A_{ext}	16.05 nm^2	Additional surface created by fibril elongation of a single monomer
$k_{m \to f}$	$-1.44 \cdot 10^{-2}\ Hz/10^9\ molecules$	Frequency change corresponding to the addition of 10^9 α-synuclein molecules
$r_{nucleate,1}$	0.1 $s^{-1}molecule^{-1}$	Rate of surface-bound monomers to find each other and form small oligomers
$r_{nucleate,2}$	0.03 $s^{-1}molecule^{-1}$	Rate at which oligomers become new fibril ends
r_{cut}	0.0025 $s^{-1}molecule^{-1}$	Rate of proteinase K cutting of the fibrils
Variable	**Initial value**	**Description**
$\Delta m(t)$	$\Delta m_0 = 0\ molecules$	Change in mass on QCM surface
$n_{full}(t)$	$n_{full,0} = 50$	Number of fibril ends with flanks
$n_{shave}(t)$	$n_{shave,0} = 0$	Number of fibril ends without flanks
$A_{free}(t)$	$A_{fibril,0} = 0\ nm^2$	Available fibril surface area
$A_{tot}(t)$	$A_{tot,0} = 401.25\ nm^2$	Total fibril surface area (based on monomers without flanks)
$m_{full\_length}(t)$	$m_{full\_length,0} = 0$	Mass added since last degradation step

To convert the change in mass to frequency of the third overtone, a factor of $k_{m\to f} = -1.44\cdot10^{-2} Hz/10^9$ molecules was used, based on existing literature[3,4].

The models were described as sets of rate equations that were solved to show the change in mass over time. Due to the elevated monomer concentrations used in the QCM-D experiments, which are more than one order of magnitude higher than in a previous study where monomer depletion was observed[4], we can assume that monomer depletion within the flow-cell can be neglected. All kinetic models assume the fibrillar core remains intact through PK treatment. Furthermore, the models assume that fibrils cannot detach from the surface.

5.2.1 Model 0: Fibril elongation with intact flanks

The null model (Fig. S11) describes the change in mass ($\Delta m(t)$) by elongation of untreated fibrils:

$$\frac{\partial \Delta m(t)}{\partial t} = r_{full} \cdot n_{full}(t) - r_{sens} \cdot \Delta m(t) \tag{S1}$$

where $\Delta m(t)$ is the change in mass, r_{full} is the growth rate of fibril with disordered flanks and $n_{full}(t)$ is the amount of fibril ends with disordered flanks. Note that in this model the number of available fibril ends remains constant ($\frac{\partial n_{full}(t)}{\partial t} = 0$) as we assume that no new fibrils are formed during fibril elongation. Additionally, the change in mass decreases slightly as $\Delta m(t)$ increases. This was included to mimic the QCM experiments, where the system loses sensitivity to newly added fibril when a lot of fibril mass is present on the QCM chip.

Since no fibril shaving takes place in this model, no mass is removed during the **shaving phase**, and thus $\frac{\partial \Delta m(t)}{\partial t} = 0$ during the **shaving phases**.

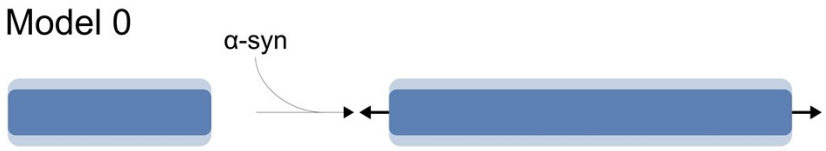

Fig. S11 Model 0, normal fibril elongation. This model describes fibril elongation under regular conditions (no flank degradation).

5.2.2 Model A: Fibril elongation without flanks

Model A (Fig. S12) assumes only elongation of fibrils after the **shaving phase**. In this model, we assume that the initial growth rate (r_{shave}) is faster than that of Model 0 (r_{full}), as incoming monomers recruited to the fibril are full length, the growth rate eventually returns to that of Model 0. During the fibril **growth phases**, the equations are as follows:

$$\frac{\partial \Delta m(t)}{\partial t} = r_{full} \cdot n_{full}(t) + r_{shave} \cdot n_{shave}(t) - r_{sens} \cdot \Delta m(t) \tag{S2}$$

where $\Delta m(t)$ is the change in mass, r_{full} is the growth rate of fibril with disordered flanks, r_{shave} is the growth rate of fibril without disordered flanks, $n_{full}(t)$ is the number of fibril ends with disordered flanks and $n_{shave}(t)$ is the number of fibril ends without disordered flanks. The change in mass is a linear combination of the number of fibril ends with and without flanks and their respective growth rates. We describe the number of fibril ends without disordered flanks as:

$$\frac{\partial n_{shave}(t)}{\partial t} = - r_{shave} \cdot n_{shave} \tag{S3}$$

The number of fibrils without flanks decreases during growth as full length monomer is recruited to the fibril. The following equation describes the number of fibril ends with intact flanks:

$$\frac{\partial n_{full}(t)}{\partial t} = r_{shave} \cdot n_{shave}(t) \tag{S4}$$

The number of fibril ends with flanks increases during growth as full length monomer is recruited to the fibril. Note that the total number of fibril ends is constant in this model, $\frac{\partial n_{shave}(t)}{\partial \partial t} = - \frac{\partial n_{full}(t)}{\partial t}$ by definition. We keep track of the amount of mass added since the last degradation

step, because this is the only part of the mass that will be affected in the next proteinase K degradation step. The newly added mass is described as:

$$\frac{\partial m_{full\_length}(t)}{\partial t} = r_{full} \cdot n_{full}(t) + r_{shave} \cdot n_{shave}(t) \quad \text{(S5)}$$

Where m_{full_length} is the amount of monomer added to the chip since the last shaving step.

During the disordered flank **shaving phase**, the equations are as follows:

$$\frac{\partial \Delta m(t)}{\partial t} = -0.3 \cdot r_{PK} \cdot m_{full\_length}(t) \quad \text{(S6)}$$

where r_{PK} is the fibril degradation rate of proteinase K. The factor of 0.3 is added because only the disordered flanks can be degraded by proteinase K, and not the entire fibril. This value matches the observed experimental behaviour.

We calculate the number of fibril ends without disordered flanks during the **shaving phase**:

$$\frac{\partial n_{shave}(t)}{\partial t} = r_{PK} \cdot n_{full}(t) \quad \text{(S7)}$$

We calculate the number of fibril ends with disordered flanks during the **shaving phase**:

$$\frac{\partial n_{full}(t)}{\partial t} = -r_{PK} \cdot n_{full}(t) \quad \text{(S8)}$$

We keep track of the total mass added to the sensor surface since the last shaving step as:

$$\frac{\partial m_{full\_length}(t)}{\partial t} = -r_{PK} \cdot m_{full\_length}(t) \quad \text{(S9)}$$

In the models, the proteinase K degradation phase is made sufficiently long until m_{full_length} =0.

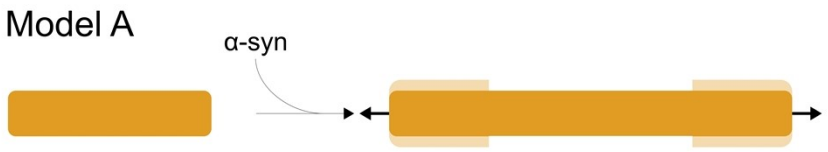

Fig. S12 Model A. This model describes fibril elongation on a fibril without disordered flanks. The initial elongation rate is higher than when flanks are present (Model 0), but will quickly return to a slower rate, since the monomers added to the fibril do have intact flanks.

5.2.3 Model B: Fibril elongation without flanks and surface binding

Model B extends Model A with description of monomers binding to the surface of the "shaven" regions of fibrils, caused by the electrostatic and steric repulsion due to the removal of the negatively charged disordered C-terminal tail of the fibrils. This surface binding does not lead to the growth of new fibrils. During the fibril **growth phases**, the equations are as follows:

$$\frac{\partial \Delta m(t)}{\partial t} = r_{full} \cdot n_{full}(t) + r_{shave} \cdot n_{shave}(t) + r_{bind} \cdot A_{free}(t) - r_{sens} \cdot \Delta m(t) \quad \text{(S10)}$$

where $\Delta m(t)$ is the change in mass, r_{full} is the growth rate of fibril with disordered flanks, r_{shave} is the growth rate of fibril without disordered flanks, $n_{full}(t)$ is the amount of fibril ends with disordered flanks, $n_{shave}(t)$ is the amount of fibril ends without disordered flanks, r_{bind} is the rate of monomer binding to the surface, $A_{free}(t)$ accessible "shaven" fibril surface area and $A_{tot}(t)$ is the total "shaven" fibril surface **Table S1**. The change in mass is a linear combination of the amounts of fibril with and without flanks and their respective growth rates plus the added mass of monomers binding to the fibril surface.

$\frac{\partial n_{shave}(t)}{\partial t}$ and $\frac{\partial n_{full}}{\partial t}$ are described as in equations Equation S3 and Equation S4, respectively.

To describe the total accessible surface area of "shaven" fibrils we use:

$$\frac{\partial A_{free}(t)}{\partial t} = -r_{bind} \cdot A_{monomer} \cdot A_{free}(t) \quad \text{(S11)}$$

Here, the total accessible surface area of the fibrils decreases over time as monomers bind to the surface. The rate of surface binding also decreases as the fraction of available surface decreases. To describe the total surface area of "shaven" fibrils we use:

$$\frac{\partial A_{tot}(t)}{\partial t} = 0 \tag{S12}$$

Since recruited monomers are full length, A_{tot} (t) does not increase during the growth phases.

$$\frac{\partial m_{full\_length}(t)}{\partial t} = r_{full} \cdot n_{full}(t) + r_{shave} \cdot n_{shave}(t) + r_{bind} \cdot A_{free}(t) \tag{S13}$$

where $m_{full\_length}(t)$ is the monomer recruited to the sensor since the last shaving step. We keep track of this separately, because during the degradation steps only the parts of fibril consisting of newly added monomers is affected.

During the **shaving phase**, the decrease in mass is described as in Model A (Equation S6). The change in number of fibrils with and without disordered flanks are described as in equations Equation S8 and Equation S7, respectively. The change in accessible fibril surface area is described as follows:

$$\frac{\partial A_{free}(t)}{\partial t} = r_{PK} \cdot \left(A_{tot}(t) - A_{free}(t)\right) + r_{PK} \cdot A_{ext} \cdot m_{full\_length}(t) \tag{S14}$$

where A_{ext} is the additional surface area created by the addition of a single monomer to the fibril end. The total available surface area increases both because the surface area bound by monomers becomes available again and from the newly added monomers to the fibril ends as the disordered flanks are degraded.

The change in total "shaven" fibril surface area is described as follows:

$$\frac{\partial A_{tot}(t)}{\partial t} = r_{PK} \cdot A_{ext} \cdot m_{full\_length}(t) \tag{S15}$$

The total surface area increases as the fibril is elongated.

The decrease in m_{full_length} is described as Equation S9.

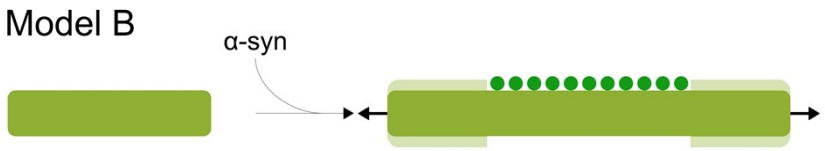

Fig. S13 Model B. This model describes fibril elongation on a fibril without disordered flanks (Model A). Additionally, in this model monomers can bind to the surface, only on the parts of the surface where no flanks are present. This surface binding does not lead to the growth of new fibrils.

5.2.4 Model C: Fibril elongation without flanks and surface binding leading to branched growth of new fibrils

Model C (Fig. S14) extends Model B by allowing branched growth of surface nucleated fibrils on the surface area of "shaven" fibrils, with a lag time to allow for both forming of small oligomers on the surface and the formation of a new fibril seed of these oligomers. During the fibril **growth phases**, the change in mass is described as in Equation S10, and the change in number of fibril ends without flanks is as described in Equation S3. The change in the amount of surface-bound fibrils is described as:

$$\frac{\partial n_{bound}(t)}{\partial t} = r_{bind} \cdot A_{free}(t) \tag{S16}$$

where $n_{bound}(t)$ is the number of bound monomers, which has the same rate of surface binding as model B. The change in the number of nuclei on the fibril surface is described as:

$$\frac{\partial n_{nucleate}(t)}{\partial t} = r_{nucleate,1} \cdot n_{bound}(t) - r_{nucleate,2} \cdot n_{nucleate}(t) \tag{S17}$$

where $r_{nucleate,1}$ is the rate at which surface-bound monomers aggregate on the surface, $r_{nucleate,2}$ is the rate at which these nuclei transition into new fibril ends, branching off the original surface. The change in the number of fibril ends with flanks is described as:

$$\frac{\partial n_{full(t)}}{\partial t} = r_{shave} \cdot n_{shave}(t) + r_{nucleate,2} \cdot n_{nucleate}(t) \quad \text{(S18)}$$

The number of fibrils with flanks increases during growth as full length monomer is recruited to the fibril end. Additional fibril ends are created because surface-bound aggregates form additional fibrils branching off the original fibril surface (secondary nucleation).

The change in available fibril surface area is described as in Equation S11, and the total amount of surface area as in Equation S12. The amount of newly added fibril is described as Equation S13.

During the **shaving phase**, the change in mass is described as in Model B (Equation S6). The change in the amount of fibril ends with and without flanks are described as in equations Equation S8 and Equation S7, respectively.

The change in the available fibril surface area is described as in Equation S14. The change in total surface area is described as in Equation S15. The change in newly added mass is described as in Equation S9

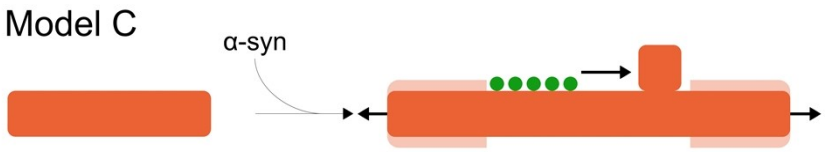

Fig. S14 Model C. This model describes fibril elongation and surface binding of monomers on a fibril without disordered flanks as in Model B. Additionally, monomer binding to the fibril surface leads nucleation of new fibrils.

5.2.5 Model D: Proteinase K digestion leads to breaking of fibrils

In Model D (Fig. S15) fibrils may be broken during the proteinase K digestion step. The new ends that are created this way can grow in the subsequent growth phase. Monomers can bind to "shaven" fibrils, but, as in model B, this does not lead to surface growth of new fibrils.

During the fibril **growth phases**, model D behaves as Model B.

During the **shaving phases**, the change in number of fibril ends without flanks is described as:

$$\frac{\partial n_{shave}(t)}{\partial t} = r_{PK} \cdot n_{full}(t) + r_{cut} \cdot \Delta m(t)$$

where r_{cut} is the rate at which the fibrils are broken up by Proteinase K. The model otherwise behaves as Model B.

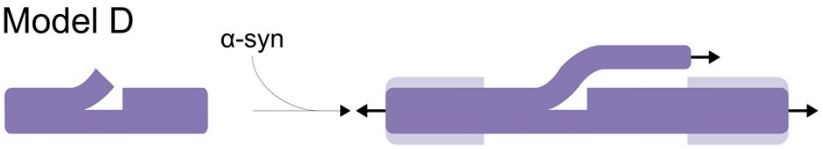

Fig. S15 Model D. This model describes fibril elongation and proteolytic fragmentation leading to the formation of new fibril ends.

Supplementary notes and references

1 M. D. Tuttle, G. Comellas, A. J. Nieuwkoop, D. J. Covell, D. A. Berthold, K. D. Kloepper, J. M. Courtney, J. K. Kim, A. M. Barclay, A. Kendall, W. Wan, G. Stubbs, C. D. Schwieters, V. M. Y. Lee, J. M. George and C. M. Rienstra, *Nature Structural & Molecular Biology*, 2016, **23**, 409–415.

2 W. G. Touw, C. Baakman, J. Black, T. A. H. te Beek, E. Krieger, R. P. Joosten and G. Vriend, *Nucleic Acids Research*, 2014, **43**, D364–D368.

3 A. K. Buell, A. Dhulesia, D. A. White, T. P. Knowles, C. M. Dobson and M. E. Welland, *Angewandte Chemie - International Edition*, 2012, **51**, 5247–5251.

4 T. C. Michaels, A. K. Buell, E. M. Terentjev and T. P. Knowles, *Journal of Physical Chemistry Letters*, 2014, **5**, 695–699.